Geochemical Journal, Vol. 40, pp. 69 to 85, 2006

Fluid inclusions and their stable isotope geochemistry of the carbonate-hosted talc deposits near the Cretaceous Muamsa Granite, South Korea

DONGBOK SHIN[1]* and INSUNG LEE[2]

[1]Mineral Resources Group, Korea Institute of Geoscience and Mineral Resources, Gajeong-dong 30, Daejeon 305-350, South Korea
[2]School of Earth and Environmental Sciences, Seoul National University, San 56-1, Shinrim-dong, Kwanak-gu, Seoul 151-742, South Korea

(*Received November 23, 2004; Accepted July 19, 2005*)

Microthermometric and stable isotope studies of fluid inclusions were conducted for the Poongjeon talc deposit which formed as alteration products of calc-silicate minerals during the retrograde stage of contact metamorphism related to the intrusion of the Cretaceous Muamsa Granite of South Korea. Two types of quartz vein are observed in the deposit. Vein I, which occurs in marble, is characterized by both mixing and unmixing process of fluid inclusions. Repeated boiling of carbonic fluids produced high X_{CO2} fluids abundantly and low X_{CO2} or aqueous fluids a little. Occasionally mixing took place between halite ± sylvite-bearing fluids and carbonic fluids. As for vein II, which occurs typically at points of amphibolite-metapelite contact, the fluid mixing model can be applied to the coexistence of abundant $CH_4 \pm H_2O$, H_2O-CO_2-CH_4 fluids with variable CH_4/CO_2 ratios ($X_{CH4} > 0.1$), and minor high X_{CO2} fluid inclusions. The CH_4-rich inclusions seem to be derived from the reheating of C-bearing metapelite during contact metamorphism.

Occurrences of halite ± sylvite-bearing inclusions along trails in both vein I and II are chronologically behind other primary inclusions and are closely related to the talc mineralization. The mineralizing fluids would have been derived directly from a water-saturated crystallizing melt and the entrapment occurred between 150 and 700 bars at 260°–390°C. The $\delta^{13}C_{CO2}$ values, 0.1–2.4‰, of inclusion fluids of vein I seem to have resulted from the isotopic exchange of magmatic carbon with ^{13}C-enriched CO_2 liberated from the decarbonation for calc-silicate formation. Distinctly lower $\delta^{13}C_{CO2}$ values, –3.5 to –1.7‰, in vein II could have originated from the strong effect of metasediment-derived fluids. Higher $\delta^{18}O_{H2O}$ values of vein I and lower δD values of vein II, both of which belong to the magmatic water range, seem to have similar evolution history as $\delta^{13}C$ values. Geologic structures such as faults and contacts between different rock units seem to have promoted infiltration, mixing, and unmixing of fluids of diverse origins.

Keywords: fluid mixing, unmixing, stable isotope, talc deposit, South Korea

INTRODUCTION

The talc deposits of South Korea can be classified into two types in relation to their host rocks: those of Mg-carbonate origin (e.g., Park *et al*., 1997) and those of ultramafic rock origin (e.g., Lee and Choi, 1994), of which the former is of greater economic importance. Most of the Mg-carbonate origin deposits are concentrated in the Ogcheon Metamorphic Belt of central South Korea. Especially, more than twenty low-grade talc deposits of Mg-carbonate origin containing a large proportion of tremolite as impurities are distributed near the Cretaceous Muamsa Granite in the Hwanggangri Mineralized Zone of the Ogcheon Metamorphic Belt (Fig. 1). They were actively mined using the open-pit methods from the 1970s to the early 1990s, and the past production and estimated reserves of the Hwanggangri Mineralized Zone are about 1.5 million tonnes of ore (KMPC, 1989). Although extensive reserves of talc may be present, the low quality of the ores, due to the abundance of tremolite, has limited large-scale development.

Park *et al*. (1997) and Shin and Lee (2000) provided the general description of the ore deposits and identified the ore mineralogy and its mineral chemistry. More recently, Shin and Lee (2002, 2003) studied the contact metamorphic process related to the granite intrusion and explained the stable isotope variations in the carbonate contact aureole, which has been subjected to fluid-rock interactions. They discussed the elemental behavior of talc ores during the mineralization process, and also tried to constrain the physicochemical parameters of the mineralization.

However, comparatively little information on the nature of mineralizing fluids makes it difficult to understand

*Corresponding author (e-mail: shin@webmail.kigam.re.kr)

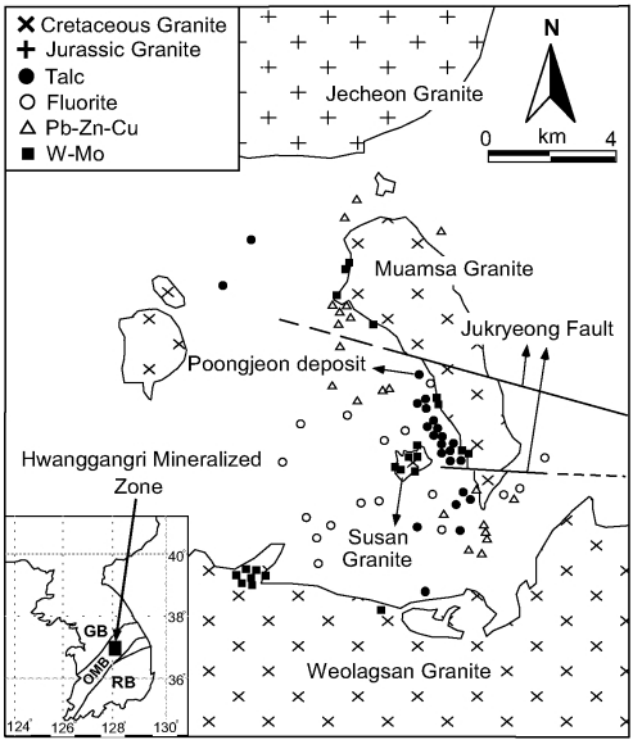

Fig. 1. Simplified geologic map showing the distribution of talc and other ore deposits near the Cretaceous Muamsa Granite in the Hwanggangri Mineralized Zone of the Ogcheon Metamorphic Belt (after Shin and Lee, 2002). GB: Gyeonggi Block, RB: Ryeongnam Block.

the relationship between granite intrusion followed by contact metamorphism and talc mineralization in view of fluid evolution. Thus, special emphasis is given to microthermometric and stable isotope characteristics of fluid inclusions in the vein quartz embedded in the ore body from the Poongjeon deposit, the most representative and largest in the mineralized area, to identify the origin and composition of the fluid and to interpret its evolutionary history during the mineralization process.

GEOLOGY AND MINERALIZATION

Geologic setting

The Poongjeon deposit is located in the northeastern Ogcheon Metamorphic Belt, which forms the boundary between two Archean to middle Proterozoic blocks, Gyeonggi to the northwest and Ryeongnam to the southeast (Fig. 1; Cluzel *et al*., 1990) and is divided into southwestern metamorphic and northeastern non-metamorphic areas. The Ogcheon Metamorphic Belt is interpreted to have undergone several metamorphic episodes, which have contributed to the formation of a fold-thrust zone that is defined by SE-verging, ductile, and stacking nappes (Cluzel *et al*., 1990). These have resulted from the deformation of Paleozoic to early Mesozoic sedimentary or metasedimentary rocks. The intrusion of Cretaceous granite, including the Muamsa Granite, extending from the southeast edge of the Ogcheon Metamorphic Belt created contact metamorphism.

The Poongjeon talc deposit is close to the western contact of the Muamsa Granite. The mine area consists of sedimentary rocks of the Cambro-Ordovician Samtaesan Formation, amphibolite, and the Cretaceous Muamsa Granite, which has intruded into the sedimentary rock sequence (Fig. 2). The Samtaesan Formation consists of pelitic hornfels, calcitic marble, metapelite and dolomitic marble in an upward sequence. Highly recrystallized and massive calcitic marble generally contains calcite, quartz, diopside, tremolite, wollastonite, and phlogopite. Metapelite intruded by amphibolite is distributed broadly in the central part of the area and bordered partly by talc ore bodies along its upper contact with the dolomitic marble. Dolomitic marble is located in the upper Samtaesan Formation of the study area. The marble is moderately recrystallized and commonly bears silicate minerals such as tremolite, diopside, forsterite, phlogopite, and serpentine. Calc-silicate rocks composed mainly of tremolite and diopside occur over a wide area around the talc ore body in the dolomitic marble, and rhythmic intercalations of thin pelitic-calcitic marble beds

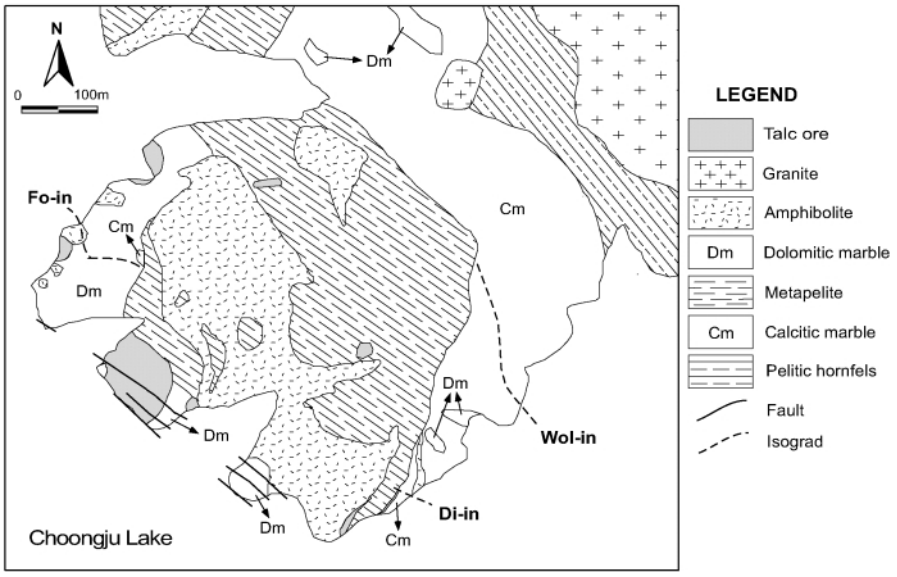

Fig. 2. Geologic map of the Poongjeon talc deposits (after Park et al., 1997; Shin and Lee, 2002). Isograds shown are based on petrographically determined assemblages and do not refer to specific reactions. Wol = wollastonite, Di = diopside, Fo = forsterite.

(<10 cm) are also observed. Successive appearances of tremolite, diopside and wollastonite in calcitic marbles, and of tremolite, diopside and forsterite in dolomitic marble are observed in the contact aureole.

Amphibolite occurs either as a massive body or as schistose planar. The former shows irregular boundaries and chilled margins along the contacts with surrounding sedimentary rocks, and fragments of metapelite occur as inclusions in the amphibolite. The Muamsa Granite has intruded into the Samtaesan Formation along a NW-SE direction to form elongated domes ≥10 km long and ≤4 km wide. The granite is typically a medium-grained, biotite granite, but its marginal portions are fine-grained, with feldspar phenocrysts displaying myrmekitic and perthitic intergrowths. In the margin of the intrusion, small (<3 mm) miarolitic cavities are commonly observed. These features indicate that the Muamsa Granite was consolidated from a water-rich magma (Newberry, 1982). The granite yields an Rb-Sr feldspar age of 109 ± 3 Ma (Jin *et al*., 1992). Geochemical studies have shown that the Muamsa Granite mostly represents K-rich, I-type granites that were highly evolved (D.I. = avg. 89.89) through fractional crystallization of calc-alkaline magma to alkaline rocks (Jin, 1985; So and Yun, 1992). Jang and Gim (1996) determined the emplacement pressure of the Cretaceous granite in the Hwanggangri area, 1 to 2 kbar, from fluid inclusion study.

Ore deposits

Talc orebodies in the Poongjeon deposit are emplaced generally in the calc-silicate rock in dolomitic marble of the upper part of the Samtaesan Formation. They were distinctly controlled by structural features such as faults, joints, or lithologic contacts between dolomitic marble and metapelite or amphibolite. The boundary between dolomitic marble and calc-silicate rock is obscure, whereas the contact of orebody with calc-silicate rock is comparatively sharp and irregular.

The main ore bodies extend 100 m in length and 80 m in thickness and are concentrated along the shattered zone created by several subvertical, N50°W-trending sets of faults which are filled with vein quartz. Orebodies are also found as centimeter- to meter-sized veins or pods of variable orientation crosscutting and replacing calc-silicate rocks. It is interpreted that the calc-silicate rocks in the dolomitic marble formed with infiltration of siliceous fluids during the prograde stage of the contact metamorphism and the talc mineralization was followed during the retrograde stage.

The calc-silicate rocks consist mainly of tremolite with minor phases of diopside and phlogopite, and interstitial phases of calcite and quartz as accessories. In the orebody talc occurs in variable proportions as alteration products of tremolite, or rarely, of diopside and phlogopite, and forms fine-grained, fibrous aggregates. No primary talc has been observed as yet. Tremolite is typically replaced partly or completely by talc, and infrequently talc forms pseudomorphs after tremolite. Quartz is included as nodular form with sizes 3~4 cm or less in the ore bodies. The ore occurs in a schistose form, showing fine-grained and fibrous aggregates, not as a compact and massive variety of steatite. The K-Ar age determined for phlogopites in-

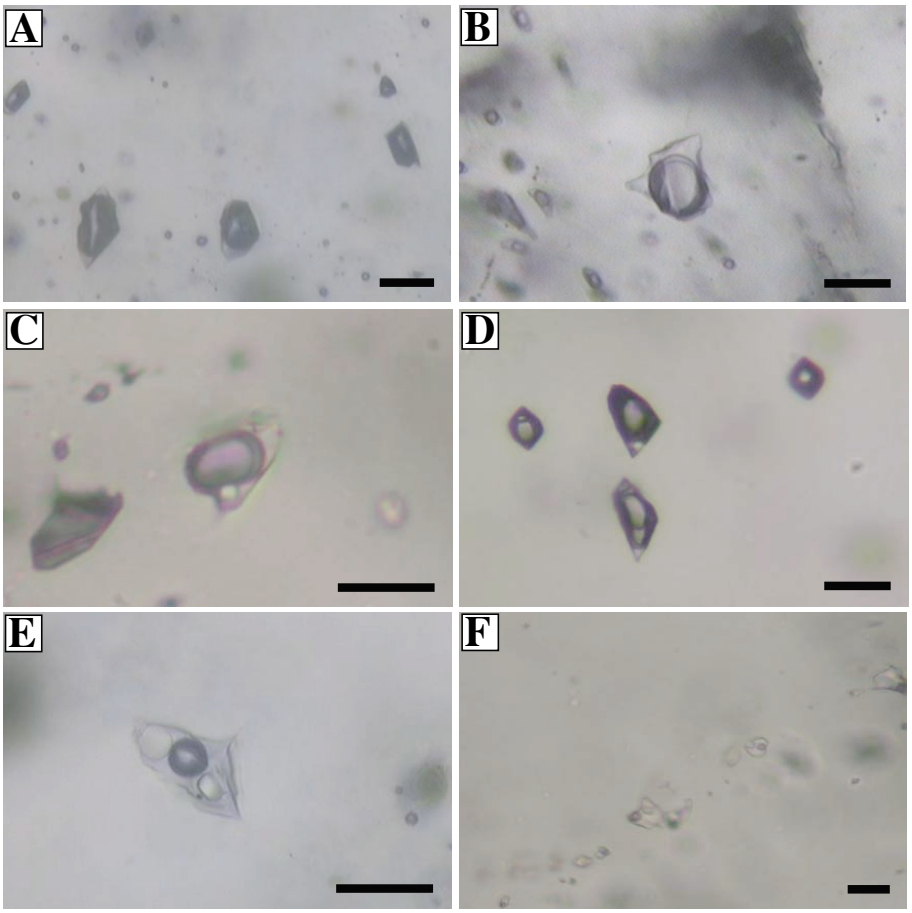

Fig. 3. Microphotographs showing the types and occurrences of fluid inclusions from the Poongjeon deposits. A: Type I inclusions typically found in vein II. B: Type IIB1 inclusions in vein I. C: Halite-bearing carbonaceous inclusions in vein I. D. Coexistence of type I and IIB2 inclusions in vein II. E: Type IV primary inclusions with halite and sylvite in the aqueous phase. F: Type IV secondary inclusions constituting linear trails. Scale bars: 10μm

cluded in the talc ores from the Poongjeon deposit is about 88 Ma (Shin and Lee, 2002), which is close to K-Ar biotite age, 90 ± 2 Ma, of the Muamsa Granite (Jin *et al*., 1992) and to whole-rock K-Ar age, 89 ± 2 Ma, of the Susan Granite (Fig. 1) (So and Yun, 1994).

Methods of Study

Microthermometric determinations on fluid inclusions were carried out on vein quartz samples included in talc orebodies. The measurements were focused on primary and pseudosecondary inclusions using a U.S.G.S.-type gas flow heating-freezing stage at Seoul National University. Stage calibration was carried out at –56.6°C (CO_2), 0.0°C (H_2O), and 340°C (H_2O) using synthetic fluid inclusion standards. Errors of these measurements were ±0.2°C at and below 0°C and ±1.5°C at 340°C, respectively. Salinity data were calculated from freezing point depression in the system H_2O-NaCl for CO_2-free, aqueous inclusions (Bodnar, 1993), from clathrate melting temperatures for CO_2-bearing inclusions (Darling, 1991), and from dissolution temperature for halite ± sylvite-bearing inclusions (Bodnar *et al*., 1989).

For stable isotope study twenty samples of vein quartz (13 for vein I and 7 for vein II) were selected for oxygen isotope compositions of vein quartz, and hydrogen and carbon isotope compositions of inclusion fluids. For oxygen isotope analysis vein quartz samples were treated with HCl to dissolve carbonate fractions and were processed by the method of Clayton and Mayeda (1963) to produce CO_2 gas.

For hydrogen and carbon isotope composition of inclusion fluids, pure quartz samples (mostly between 1–2 g) were heated to 150°C overnight to release volatiles and then heated above 800°C to extract the fluids in an evacuated quartz tube which is linked to a vacuum line that was designed to separate H_2O, CO_2 and CH_4 of the extracted fluids. Hydrogen isotope analyses were con-

ducted for both the prograde and retrograde stage fluids. To this purpose, a detailed petrographic study was carried out to select the appropriate samples that would minimize the percentage of other stage inclusions.

Measurement for oxygen isotope composition was conducted using the Finnigan MAT 252 with dual-inlet mass spectrometer at Indiana University with analytical precision of better than ±0.1‰. Carbon and hydrogen isotope compositions were measured on a VG Isotech PRISM II spectrometer at the Korea Basic Science Institute. The analytical precision of both $\delta^{18}O$ and $\delta^{13}C$ measurements is within ±0.1‰ and better than ±1.0‰ for D/H analysis. Oxygen and hydrogen isotope data are expressed relative to SMOW, and carbon isotope data relative to PDB.

Fluid Inclusion Studies

Petrography of fluid inclusions

The examined quartz samples are inclusion-rich, probably due to repeated fracturing and healing. Petrographic study and subsequent single inclusion measurements were focused on closely associated groups or trails of inclusions with visually identical phase ratios and similar shape. Inclusion sizes generally vary from <5 to >30 μm. Fluid inclusions can be classified into four types (Fig. 3) based on the number of phases, degree of filling at room temperature, and phase variations during heating and freezing experiments. Though the repeated fracturing and healing, both during and after quartz precipitation, make it difficult to distinguish primary and secondary inclusions, the presence of inclusions in growth zones or along fracture planes, in some cases, however, enables the establishment of a relative chronology of inclusions using Roedder's criteria (1984). Microthermometric as well as petrographic studies identified two different types of quartz veins showing different assemblages of fluid inclusions: one from the marble or the marble-amphibolite contact (vein I) and the other from the amphibolite-metapelite contact (vein II).

Type I inclusions contain $CH_4 \pm H_2O$ fluids and are typically found in vein II. They consist of a single, supercritical bubble phase and a variable aqueous phase (Fig. 3A). The bubble generally occupies 40 to 90% of the inclusions by volume and sometimes the inclusions are nearly free of water. These inclusions show negative crystals or irregular shapes with sizes reaching over 20 μm. They are randomly distributed or sometimes occur as trails showing primary or pseudosecondary features in origin.

Type II inclusions are H_2O-CO_2-CH_4 fluids and are quite abundant in most samples. Carbonic phases homogenize to vapor phase in the inclusions, and they are further classified into subtypes based on their total homogenization mode, either to liquid (IIA) or vapor (IIB) (Fig.

Table 1. Summary of microthermometric data of fluid inclusions

Inclusion type	Homogenization mode	Composition	Tm(carb) (°C)	Tm(clath) (°C)	Th(carb) (°C)	Tm(ice) (°C)	Th(total) (°C)	Salinity (wt.% NaCl eq.)
Type I	V	$CH_4 \pm H_2O$	−183.4~−179.6	10.2~18.8	−83.5~−71.8		318~377	
Type II		H_2O-CO_2-CH_4						
IIA	L		−57.7~−57.2	4.5~7.1	23.6~25.3		343~356	5.5~9.7
IIB1	V	$X_{CH4} < 0.1$	−59.7~−56.7	4.2~9.7	22.4~28.5		312~397	1.8~10.2
IIB2	V	$X_{CH4} > 0.1$	−69.5~−59.8	5.4~14.3	−54.8~7.0		312~386	?
Type III	L	H_2O-NaCl				−15.1~−7.5	318~388	11.1~18.7

Inclusion type	Homogenization mode	Composition	Stage	Tm(halite) (°C)	Th(vapor) (°C)	Salinity (wt.% NaCl eq.)	(K/Na)atomic	
Type IV-A	Tm(halite) < Th(vapor)	H_2O-NaCl-Halite	Primary	359~374	381~388	42~44		
			Secondary	101~242	189~251	28~34		
Type IV-B	Tm(halite) > Th(vapor)	H_2O-NaCl-Halite ± Sylvite	Primary	271~447	146~388	36~69	0.54~1.38	
			Secondary	154~352	139~262	30~43	0.35~1.56	

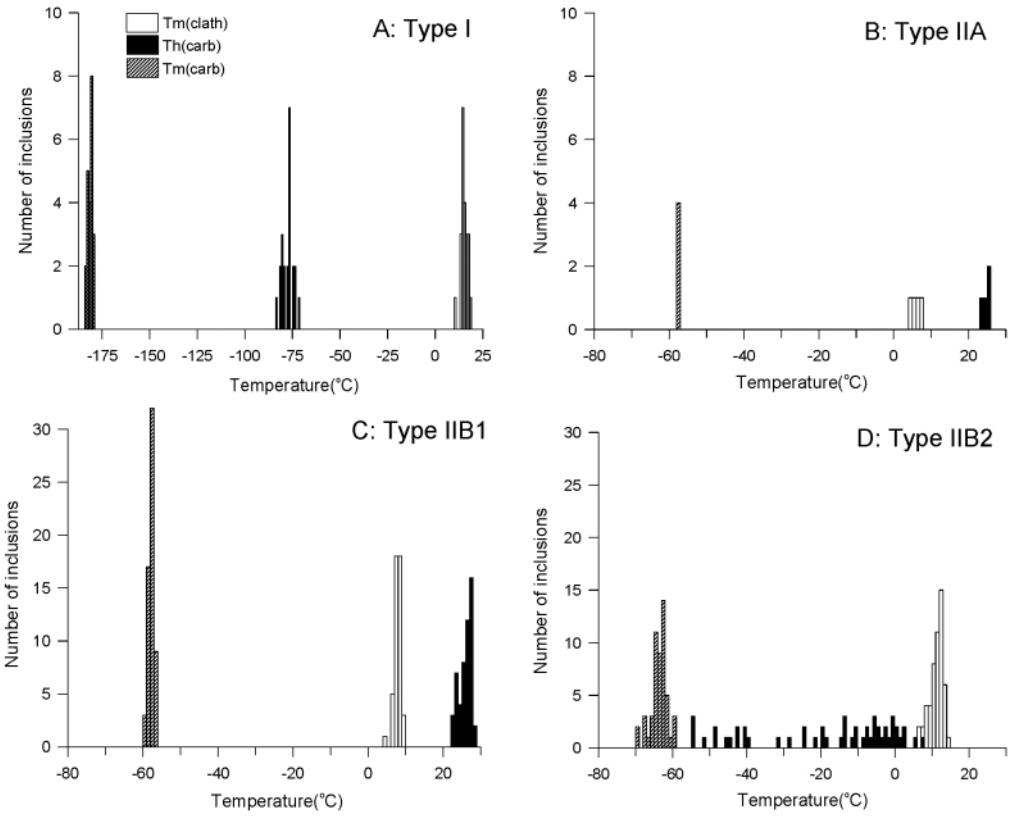

Fig. 4. Histograms of microthermometric measurements of Tm(carb), Th(carb), and Tm(clath) for type I and II fluid inclusions.

3B). Depending on CH_4 concentration in the carbonic phase, type IIB inclusions are subdivided into type IIB1 with $X_{CH4} < 0.1$ and type IIB2 with $X_{CH4} > 0.1$. Type IIB1 fluid inclusions are major constituents in vein I embedded in the marble or at the contact between marble and amphibolite. Very rarely, halite-bearing type IIB1 inclusions are also observed (Fig. 3C). Type IIB1 inclusions usually occur as clusters or are randomly distributed together with type IIA or type III inclusions in vein I. Meanwhile, most type IIB2 inclusions occur together with type I (Fig. 3D) and less commonly with type IIB1 inclusions in vein II. They occur either as clusters or in linear arrays, and do not crosscut quartz grains.

Type III inclusions are liquid-rich, aqueous inclusions consisting of a liquid and a vapor phase with a filling degree of 60 to 80 vol.% and commonly display round to negative crystal forms with sizes reaching over 20 μm. The liquid-rich inclusions do not contain daughter minerals and homogenize to liquid phase upon heating. They are randomly distributed or occur as clusters in vein I, and are commonly visible with CO_2-bearing type II inclusions, indicating the possible coeval trapping of these inclusions.

Type IV inclusions are liquid-rich and consist of aqueous liquid, vapor, and solid phases, such as halite and sylvite, at room temperature (Fig. 3E). They are found both in veins I and II. Most solid phases were dissolved during heating experiments and are regarded as daughter minerals. The vapor phase generally occupies about 10–20 vol.%. The inclusions can be further divided into two subtypes based on their homogenization mode. In type IVA inclusions, solid phases are dissolved first and the disappearance of vapor bubbles follows, while in type IVB inclusions, vapor bubbles disappear first and then, total homogenization is established by solid phase dissolution. Some type IV inclusions are found in clusters or isolated domains showing primary features and sometimes bounded by carbonic inclusions. Others constitute linear trails and often crosscut the populations of type I, II, or III inclusions, representing pseudosecondary or secondary origins (Fig. 3F). Most of the inclusions show irregular shapes with variable sizes and occasionally form negative crystals.

As described above, the distinct difference between the two vein types lies in the occurrence of CO_2-rich inclusions in vein I and CH_4-rich inclusions in vein II, while hypersaline fluid inclusions are common in both of the vein types.

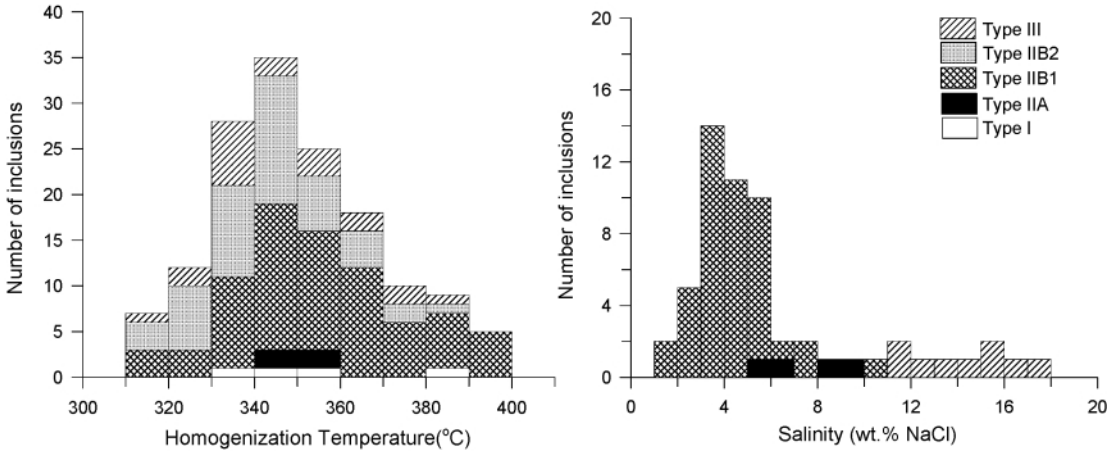

Fig. 5. Histograms of microthermometric measurements of type I, II, and III fluid inclusions. A: Homogenization temperatures, B: Salinities.

Microthermometric results

The microthermometric data of fluid inclusions are summarized in Table 1 and demonstrated in Figs. 4 to 9. Low-temperature phase changes were measured first to minimize the possibility of decrepitation of the inclusions during heating experiments. The following salinity data are expressed in weight percent of NaCl equivalent. The wide range of fluid compositions and homogenization temperatures of fluid inclusions in quartz probably reflects several hydrothermal episodes rather than one specific event, as indicated by textural evidence of multiple fracturing.

In type I inclusion, CH_4-rich inclusions create a vapor bubble when the temperature is lowered to about –100°C. A solid phase formed when the inclusion is cooled down to the temperature of liquid nitrogen, and upon heating, melts very quickly between –183.4° and –179.6°C, which is near the triple point temperature of pure CH_4 at –182.5°C (van den Kerkhof and Thiery, 1994).

Homogenization of carbonic phases into liquid bubble or through critical behavior occurs between –83.5° and –71.8°C, most of which are above the critical temperature of CH_4 (–82.6°C), indicating the presence of minor amounts of CO_2, but negligible amounts of N_2. High clathrate melting temperatures between 10.2° and 18.8°C are related with the inclusions that show critical behavior in their carbonic phases. This relationship is consistent with the results of Seitz and Pasteris (1990), which demonstrated that the critical isochore for CH_4 intersects the decomposition boundary for CH_4 clathrate at 19°C, and also showed that the clathrate melting temperature increases sharply with increasing pressure, i.e., increasing density. Most inclusions, especially those with large bubble volumes, were decrepitated before total homogenization was reached.

In type IIB1 inclusion, homogenization of the carbonic phase to vapor occurs from 22.4° to 28.5°C, corresponding to low CO_2 density between 0.21 and 0.30 g/cc. The variation of Th-CO_2 values within a single quartz grain indicates that the density of the CO_2-phase varied during the entrapment of the fluids.

Tm(carb) values of type IIB2 inclusions are much lower than type IIB1 inclusions, and Tm(clath) values, 5.4° to 14.3°C, are mostly higher than the expected temperature of pure H_2O-CO_2 fluids, 10°C. The variations of Tm(carb) and Th(carb) within a given sample indicate the variations of CH_4 concentration and carbonic phase ($CO_2 + CH_4$) density during the entrapment, although the inclusions have a uniform shape within most individual clusters. Many of the type IIB inclusions were decrepitated ahead of total homogenization due to high internal pressures related to their high carbonic content (Burrus, 1981).

Plots of low temperature behavior of the aqueous and carbonic portions of type II inclusions are shown in Figs. 6 and 7. A positive correlation between Tm(carb) and Th(carb) values (Fig. 6), and a negative correlation between Tm(carb) and Tm(clath) values (Fig. 7) are evident. Tm(carb) for type II inclusions lower than –56.6°C, which is expected for pure CO_2, indicates the presence of CH_4 in the inclusion fluids (Burrus, 1981). The amounts of CH_4 in the carbonic phase can be estimated from the relationship between Tm(carb) and Th(carb) using the data of Thiery *et al.* (1994) (Fig. 6), assuming that the phase responsible for the depression of the Th(carb) was CH_4. The results show that most of the type II inclusions from vein I are less than 0.1 in X_{CH4}, while most type II inclusions from vein II are above 0.1 in X_{CH4}.

As the input of CH_4 to the H_2O-CO_2-NaCl system adds a new compound, CH_4 clathrate hydrate, which is com-

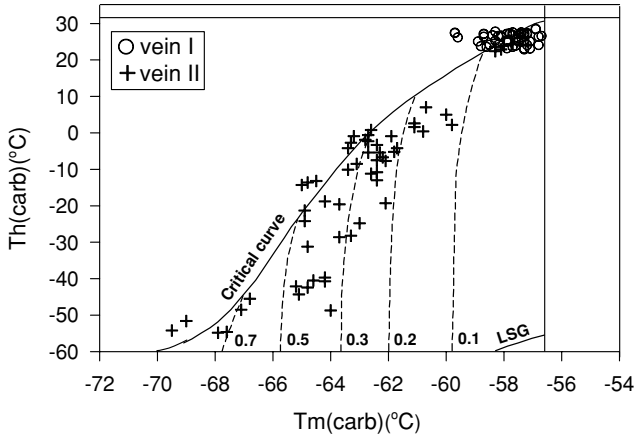

Fig. 6. Tm(carb) vs. Th(carb) diagram for H_2O-CO_2-CH_4 fluid inclusions in vein quartz. Contours of X_{CH4}, critical curve, and liquid-solid-gas (LSG) univariant curve constructed assuming homogenization to the liquid from figures in Thiery et al. (1994). Solid lines at –56.6°C and +31.9°C represent the melting point and critical point of pure CO_2, respectively. Tm(carb) values above the critical curve may indicate the presence of small amounts of a third component in the carbonic phase.

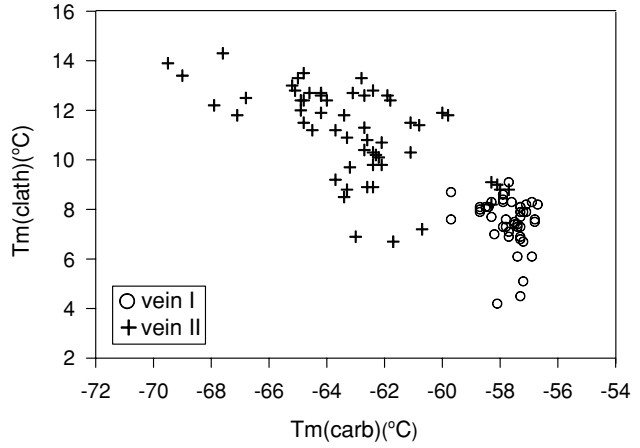

Fig. 7. Tm(carb) vs. Tm(clath) diagram for H_2O-CO_2-CH_4 fluid inclusions in vein quartz.

pletely miscible with CO_2 clathrate and complicates the interpretation of the clathrate melting phenomenon, the presence of significant amounts of CH_4 can bring about profound effects on salinity (Collins, 1979). However, if we neglect the presence of low concentrations of CH_4, less than 0.1 mole fraction, in type IIA and IIB1, the salinities are calculated as shown in Table 1.

The actual salinity for these inclusions may be higher due to the effect of methane content on the clathrate melting temperatures, because increasing X_{CH4} in the system H_2O-CO_2-CH_4 makes CO_2-CH_4 clathrate hydrate melt at

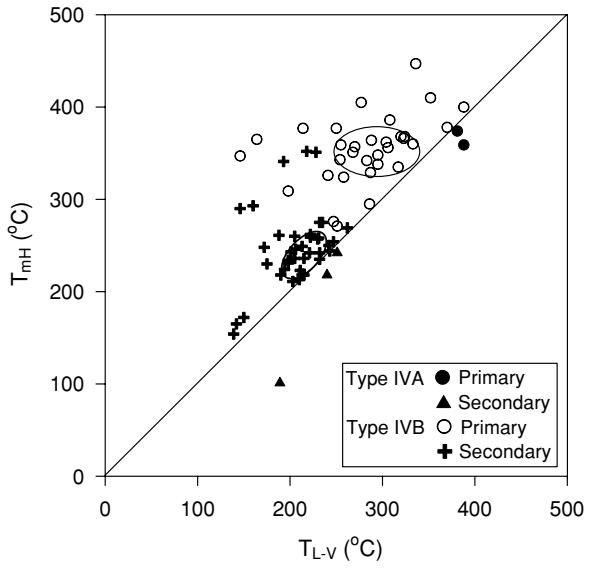

Fig. 8. Diagrams showing vapor disappearance temperatures versus halite dissolution temperatures for type IV inclusions. Two dense clusters are selected for representative temperature conditions of primary and secondary inclusions.

a temperature higher than pure CO_2 clathrate (10°C), while the addition of an NaCl component to the system should lower Tm(clath) values (Diamond, 1992). That aspect also explains why most of type IIB2 inclusions have Tm(clath) above 10°C. Furthermore, Th(carb) values of most type IIB2 inclusions are lower than Tm(clath), which is also ascribed to the presence of much CH_4 in the fluid inclusions (Burruss, 1981). Unlike type IIA and type IIB1 fluid inclusions, the salt contents of the aqueous portion of type IIB2 inclusions cannot, therefore, be simply derived from the clathrate melting temperature due to the presence of much CH_4.

During freezing runs for type III inclusions, phase changes, which are indicative of the presence of N_2 or carbonic compounds, were not observed. In most type III inclusions, the initial melting begins above –21.2°C, H_2O-NaCl eutectic temperature, suggesting that the solution is Na-rich and that other cations such as Ca^{2+} and Mg^{2+} are unimportant.

For type IV inclusions, more than 90% of the analyzed inclusions belong to type IVB in which final homogenization is established by halite dissolution. Only a few inclusions of type IVA were observed during the experiments (Fig. 8). For halite + sylvite-bearing inclusions, all of which belong to type IVB, the first phase change is either sylvite melting or vapor disappearance. The calculated total salinities in Table 1 are not corrected for the effect of other salts, such as $MgCl_2$, $FeCl_2$, and $CaCl_2$, which may well be present.

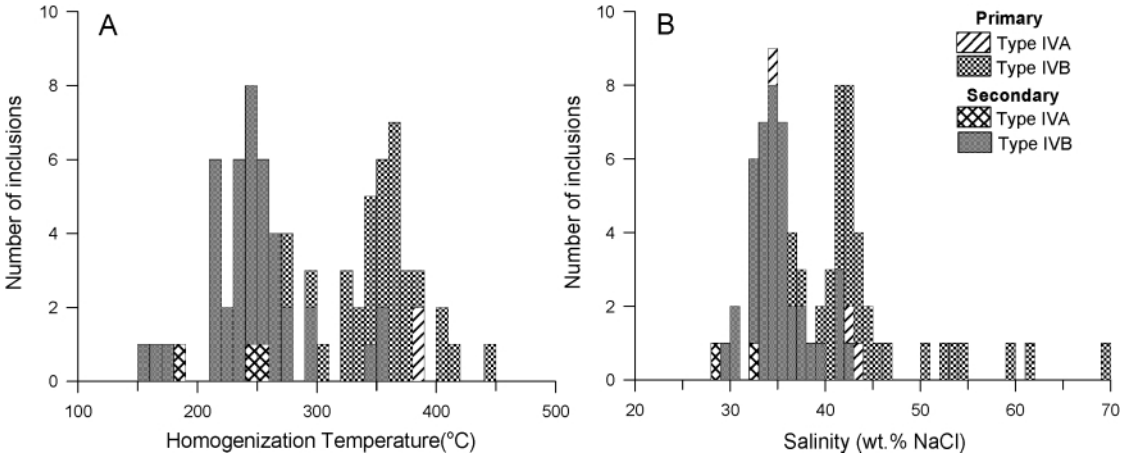

Fig. 9. Histograms of microthermometric measurements of type IV fluid inclusions. A: Homogenization temperatures. B: Salinities.

Chronological order of fluid inclusions and talc mineralization

Based on the petrographic and microthermometric study for fluid inclusions, the paragenetic sequence of fluid inclusions can be divided mainly into two stages. The first stage was initiated by the infiltration of highly saline aqueous fluids which formed type IV inclusions that are clustered in quartz grains. CO_2 and/or CH_4-bearing carbonic inclusions, type I and II, and aqueous inclusions of moderate to low salinity, type III, are major constituents of the first stage. Even though all of these inclusions display the characteristic features of primary inclusions, the occurrence of some primary type IV inclusions as isolated arrays surrounded by carbonic fluid inclusions suggests that highly saline fluids would have been coeval with or preceded carbonic fluids. High homogenization temperatures of some type IV inclusions, even above 400°C, also support this interpretation.

As described above, talc mineralization began with the formation of calc-silicate rocks by introducing silica component into the marble during the prograde metamorphic stage which was induced by the intrusion of the Muamsa Granite. Thus, in addition to the highly saline type IV inclusions, the occurrence of CO_2-rich fluid inclusions of type II seems to be the result of the decarbonation of calc-silicate formations typically exemplified by the following reactions:

$$5\ \text{dolomite} + 8\ SiO_2 + H_2O = \text{tremolite} + 3\ \text{calcite} + 7\ CO_2 \quad (1)$$

$$\text{tremolite} + 3\ \text{calcite} + 7\ SiO_2 = 5\ \text{diopside} + 3\ CO_2 + H_2O. \quad (2)$$

The second stage is characterized by the infiltration of highly saline but typically low-temperatured, generally below 270°C, aqueous fluids that form trails. No observable amounts of carbonic components seem to be involved during this stage. Shin and Lee (2002) explained that talc formation after tremolite in the calc-silicate rock is characterized by a loss of Ca^{2+} with an addition of Mg^{2+} displaying abundant fluid infiltration of igneous origin without decarbonation during the retrograde metamorphic stage, and that the immaturity of talc growth resulted from the rapid diffusion of mineralized fluids, causing instantaneous nucleation of crystals. The relationship was proposed by the following reaction, which is known as "uralitization" (Turner, 1935).

$$Ca_2Mg_5Si_8O_{22}(OH)_2 + Mg^{2+} + 2\ H^+ = 2\ Mg_3Si_4O_{10}(OH)_2 + 2\ Ca^{2+}. \quad (3)$$

Therefore, in view of the paragenetic sequences of minerals and fluid inclusions and of the properties of fluid composition, talc mineralization seems to be related to the second stage aqueous fluid infiltration that is poor in carbonic components.

Infiltration of hypersaline brine

Microthermometric characteristics of type IV fluid inclusions, which have high salinities up to 69 wt.% and high homogenization temperatures up to 447°C, are similar to those reported for other intrusion-related deposits (e.g., Roedder, 1984; Selby *et al*., 2000). In additions, pretty high K/Na ratios of about 0.9 could be derived from the equilibrium of a fluid with a granite magma (Burnham and Ohmoto, 1980).

The trapping of highly saline fluids and the presence of a high temperature metasomatic assemblage of wollastonite ± diopside in the marble near the faults or the geologic contacts of different rock units, which served as channels for the mineralizing fluids, at distances of up

to 700 m or more from the granite contact, clearly indicate that there was significant hydrothermal activity during the contact metamorphism.

Characteristically, abundant occurrences of type IVB inclusions, of which the total homogenization occurs by halite dissolution, indicate that the hypersaline fluids may have been derived directly from a water-saturated crystallizing melt (Cline and Bodnar, 1994). Further discussion about this kind of fluids follows.

Two chemically different hydrothermal fluids of different vein groups

Microthermometric measurements for fluid inclusions revealed that the spatially separated two quartz vein groups, vein I and vein II, are also chemically different. Vein I from the marble, which accounts for the main talc mineralization in the Poongjeon deposit, contains CO_2-rich fluid inclusions abundantly (type IIA, type IIB1) accompanying a small amount of CH_4 and CO_2-free aqueous inclusions (type III). CH_4-rich type I inclusions and type IIB2 inclusions are comparatively rare, suggesting that only small amounts of CH_4 were introduced during the formation of this vein. Halite ± sylvite-bearing type IV inclusions of prograde and retrograde stages are common in this quartz.

The fluid inclusions trapped in vein II, which is at the contact of amphibolite-metapelite and of little importance in view of talc mineralization, consist mainly of CH_4 ± H_2O (type I) and H_2O-CO_2-CH_4 (type IIB2) inclusions, suggesting that, unlike vein I, CH_4 is a major component. Type IIA, IIB1 and III inclusions are much less common in vein II than in vein I, while type IV inclusions are still abundant.

Origin and evolution of CH_4-rich fluid

It is uncommon to find significant amounts of CH_4 gas in silica-supersaturated igneous fluids (Roedder, 1984). Especially, a high concentration of CH_4 in type I and type IIB2 inclusions is hardly suggestive of magmatic origin, even though CH_4 is a volatile expected in a reducing magma that gives rise to S-type granitic rocks (Ishihara, 1981).

So far it has been reported that CH_4-rich fluids are commonly associated with hydrothermal fluids circulating metasedimentary rocks (e.g., Fan *et al*., 2000; Rios *et al*., 2003). The sedimentary rocks containing reduced organic matter produce aqueous fluids with $CH_4 > CO_2$ at low oxygen fugacity, while metamorphism of carbonaceous rocks can drive off aqueous fluids with $CO_2 > CH_4$ (Ferry and Burt, 1982). The Ogcheon Metamorphic Belt has experienced several times of regional metamorphisms with the peak metamorphic episode in the Middle Paleozoic followed by Late Paleozoic to Early Mesozoic metamorphic events (Cluzel *et al*., 1990). These preceded the intrusion of the Cretaceous granite, which induced decarbonation and talc mineralization in the study area. It is inferred that during the metamorphic events before the granite intrusions, most of the CH_4-rich fluids could have been generated by interaction between metamorphic fluids and organic materials, e.g., graphite, present in the sedimentary rocks, and subsequently discharged out of the system. Consequently, the local production of CH_4-rich fluids possibly originated from a fluid-rock interaction between organic materials, which survived the previous metamorphic events in the metapelite, and circulating magmatic fluid from the nearby Muamsa Granite.

Mixing and unmixing of hydrothermal fluids

Petrographic evidences and microthermometric results reveal that type IIA and IIB1 inclusions in vein I were generated by fluid unmixing, because these two types of inclusions coexist with each other in the same domains or regions, and show similar ranges of homogenization temperatures (>310°–400°C) but with different homogenization modes to either the liquid (IIA) or the vapor (IIB1). In addition, there is also a differentiation, though not distinctly, in their CO_2 mole fractions, 0.05–0.07 for type IIA and 0.20–0.64 for type IIB1. Considering that CO_2 phases are not observed in either the freezing or heating experiments under $X_{CO2} < 0.05$ in aqueous inclusions, type III inclusions, which coexist with type IIA and IIB1 inclusions with similar homogenization temperatures, could also be genetically allied with type IIA during the unmixing process. Furthermore, it is noteworthy that estimated salt contents are higher in more aqueous inclusions, type IIA (avg. 7.5 wt.%), than type IIB1 inclusions (avg. 4.5 wt.%). It is because fluid immiscibility causes solutes to be partitioned preferably into the aqueous phase rather than into the CO_2-rich vapor phase (Bowers and Helgeson, 1983b).

It is also observed that CO_2-rich inclusions of type IIA and IIB1 described above occur together not only with halite-bearing aqueous inclusions but also, though rarely, with halite-bearing carbonic inclusions. The co-occurrence of two chemically contrasted types of fluid inclusions, hypersaline aqueous fluids and CO_2-rich inclusions, has been reported by several researchers (e.g., Anderson *et al*., 1992; Fu *et al*., 2003), and generally either fluid mixing or unmixing, or sometimes both of these processes have been proposed as causes for their formation mechanisms. However, if we explain the formation of halite-bearing carbonic inclusions by the unmixing process of primeval fluids, their homogenization temperatures should be, according to Bowers and Helgeson (1983a), above 400°C at 200 bars or above 500°C at 350 bars at salinity of 6 wt.% NaCl of parental fluid, which are pretty high temperatures but low pressures. Four of these inclu-

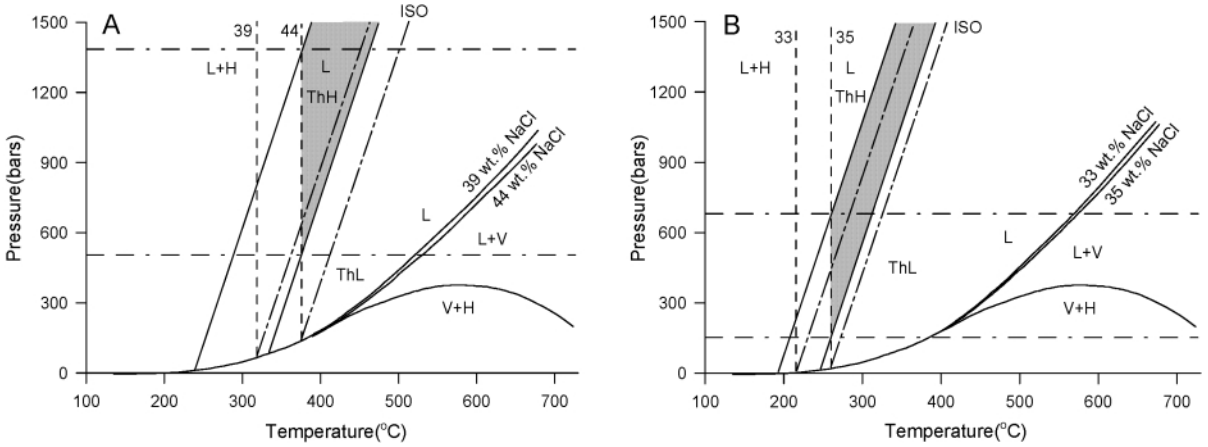

Fig. 10. Pressure-temperature diagram illustrating trapping conditions of type IVB fluid inclusions. Diagram A shows the P-T conditions of trapping of primary type IVB inclusions which are represented by liquid-vapor homogenization between 240° and 335°C and halite melting between 320° and 375°C. These inclusions have salinities of 39 to 44 wt. percent NaCl. Diagram B shows the P-T conditions of trapping of secondary type IVB inclusions which are represented by liquid-vapor homogenization between 195° to 245°C and halite melting between 215° and 260°C. These inclusions have salinities of 33 to 35 wt. percent NaCl. Isochore (ISO) divides the liquid-stable field into two subfields: fluid inclusions that homogenize by halite dissolution (ThH) and those that homogenize by vapor bubble disappearance (ThL). Shaded areas represent the typical trapping conditions of each stage of type IVB inclusions.

sions were attempted to measure homogenization temperatures, but all of them were decrepitated at temperatures above 250°C. The estimated pressure conditions of 320–480 bars for trapping of type IIA and IIB1 inclusions are somewhat higher for the formation of the halite-bearing carbonic inclusions in regard to temperature conditions.

More important thing is the common occurrence of type IVB inclusions that homogenize by halite dissolution rather than by vapor disappearance in the Poongjeon deposit. This requires the inclusions to have been trapped in the liquid-stable rather than liquid-vapor stable field, and thus could hardly be a product of fluid immiscibility (Cline and Bodnar, 1994). In additions, the occurrence of some primary type IV inclusions, which are bounded by carbonic inclusions and have higher homogenization temperatures, makes fluid immiscibility unlikely for the formation of halite-bearing carbonic inclusions.

Thus, it would be contentious to ascribe the formation of the halite-bearing carbonic inclusions which coexist with the CO_2-rich inclusions and halite-bearing aqueous inclusions to the unmixing process in the Poongjeon deposit. Instead, the occurrences seem to be more appropriately explained by the partial mixing and heterogeneous trapping of two originally unrelated, partially miscible, end-member fluids in the system of H_2O-CO_2 and H_2O-NaCl-KCl as previously discussed by Tritlla and Cardellach (1997) and Molnar *et al*. (1999).

There is a different feature in vein II. The wide variation of CH_4/CO_2 ratios or X_{CH4} in the H_2O-CO_2-CH_4 inclusions of type IIB2 inclusions ($X_{CH4} > 0.1$) (Fig. 6) can be produced by the mixing of co-existing $CH_4 \pm H_2O$ inclusions (type I) and H_2O-CO_2-CH_4 inclusions ($X_{CH4} <$ 0.1, type IIB1). Although their coexistence with similar homogenization temperatures can be used as evidences for phase separation in a mixed H_2O-CO_2-CH_4 fluid, the fluid mixing seems to be more suitable for interpretation, considering that there were originally two-end member fluids that have different generations, CH_4-rich fluids from the metasedimentary rocks and CO_2-rich fluids from the nearby marble, and that type I inclusions occur dominantly compared to type IIB1 in vein II.

Estimation of trapping conditions for fluid inclusions

Figure 8 illustrates the liquid-vapor homogenization temperatures against the halite dissolution temperatures of type IV inclusions. Two dense clusters of data are arbitrarily selected for representative temperature conditions of primary and secondary inclusions: 240°–335°C of liquid-vapor homogenization and 320°–375°C of halite dissolution for primary inclusions, and 195°–245°C of liquid-vapor homogenization and 215°–260°C of halite dissolution for secondary inclusions. To evaluate the trapping conditions of the type IV inclusion system, L + H/L boundaries for fluids with salinities of 39 and 44 wt.% NaCl for primary inclusions (Fig. 10A) and for fluids with salinities of 33 and 35 wt.% NaCl for secondary inclusions (Fig. 10B) are drawn as vertical lines.

The overlapping pressure-temperature trapping conditions for inclusions in the data cluster of Fig. 8, which

Table 2. Oxygen isotope data of vein quartz, and hydrogen and carbon isotope data for inclusion fluids from the Poongjeon deposits

Sample No.	$\delta^{18}O_{qtz}$ (‰)	δD_{H2O} (‰)		$\delta^{13}C_{CO2}$ (‰)	$\delta^{18}O_{H2O}$ (‰)**
		prograde	retrograde*		
Vein I					
PJF-1	13.8	–69		0.3	9.6
PJF-2	14.1	–70		0.3	9.9
PJF-6	15.0				10.7
PJF-7	14.4			0.1	10.1
PJF-8	15.2		–67		11.0
PJF-9	14.4	–73		1.6	10.2
PJF-10	16.2	–72		2.4	11.9
PJF-12	17.9	–68		1.3	13.7
PJF-13	14.0	–76			9.8
PJF-14	14.8		–68	0.3	10.5
PJF-15	15.8		–69		11.6
PJF-20	14.1	–70		0.8	9.9
PJF-23	15.8		–73	1.8	11.5
Vein II					
PJF-3	14.3	–82		–3.5	10.1
PJF-4	14.7				10.5
PJF-5	14.3				10.1
PJF-11	15.2	–80		–2.2	10.9
PJF-16	13.5	–78		–1.7	9.2
PJF-17	13.4	–86		–3.0	9.2
PJF-18	13.3	–82		–2.3	9.1

Abbreviation: qtz = quartz.
**For quartz veins with predominant population of secondary type IV inclusions; all other data are for the fluids of prograde stage.*
***Calculated oxygen isotope compositions based on quartz-water fractionation equation from Zheng (1993) at estimated trapping temperature of primary type IV fluid inclusions.*

exhibit halite dissolution at 320° and 375°C, are indicated by the shaded area in Fig. 10A. This represents the smallest space that could produce all fluids trapped by inclusions contained in the dense cluster for primary type IVB inclusions. The indicated minimum trapping pressure is about 500 bars (Fig. 10A), and the corresponding trapping temperatures for the selected data cluster range from 375° to 460°C, assuming a pressure range of less than 1400 bars. As for secondary type IVB inclusions, Fig. 10B illustrates that the inferred trapping temperatures for the dense cluster range from 260° to 315°C in an assumed pressure range of 150 to 700 bars.

For carbonic fluid inclusions of type IIA and IIB1 in vein I, which were produced from the unmixing process, the formation pressure can be calculated from the state function of fluid using the data of Bowers and Helgeson (1983a, b), and the results are between 320 and 480 bars. As the addition of CH_4 to H_2O-CO_2-NaCl fluid could raise the solvus toward higher pressure (Bowers and Helgeson, 1983a), the pressures given above are minimum estimates.

Thus, we believe that progressive pressure decrease occurred from the prograde hypersaline stage, 500–1400 bars, through the carbonic stage, 320–480 bars, and finally, to the retrograde hypersaline stage, 150–700 bars. The estimated pressures of primary type IV inclusions correspond to depths of about 1.9 to 5.3 km, assuming a lithostatic system that would have been subjected to fracturing induced by overpressuring of the system. Inasmuch as evidences for immiscibility were observed in type II inclusions, it is likely, though not required, that they were under hydrostatic pressure. The estimated trapping depths of these inclusions would be about 3.1 to 4.8 km, which is similar to the depth range for primary type IV inclusions, even though the depths for type II inclusions could be greater if active immiscibility decreased the bulk density of the solution with abundant vapor bubbles. According to the calculated pressure conditions, the trapping depths of secondary type IVB inclusions became shallower up to 1.5 km in a hydrostatic system.

STABLE ISOTOPE STUDIES

So far, stable isotope studies for the Poongjeon deposit have been performed on the carbonate and calc-silicate rocks in respect to the contact metamorphism and talc mineralization (Shin and Lee, 2002, 2003). This study

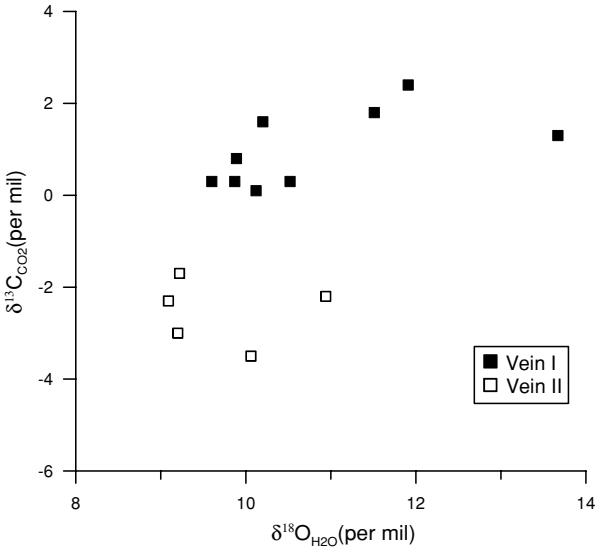

Fig. 11. Carbon and oxygen isotope diagram for fluid inclusions in two types of quartz veins from the Poongjeon deposits. $\delta^{13}C$ values are for CO_2 extracted from fluid inclusions and $\delta^{18}O$ values are for water equilibrated with quartz.

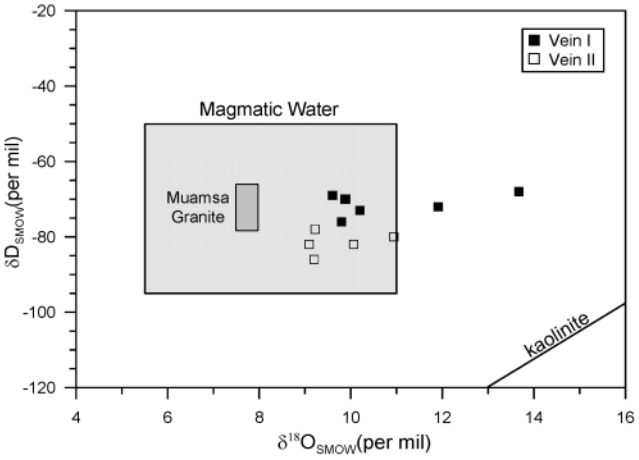

Fig. 12. δD and $\delta^{18}O$ cross plot of primary fluid inclusions in two types of quartz veins from the Poongjeon deposits. Oxygen isotope compositions are $\delta^{18}O$ values of water equilibrated with quartz which was calculated using the estimated trapping temperature of primary type IV fluid inclusions. Oxygen and hydrogen isotope compositions of the Muamsa Granite (Shin and Lee, 2003) and common magmatic water (Taylor and Sheppard, 1986) are shown together.

focuses mainly on stable isotope characteristics of fluid inclusions to elucidate the origins and evolutionary history of hydrothermal fluids related to talc mineralization.

Stable isotope compositions

The stable isotope values for oxygen, hydrogen and carbon are listed in Table 2. The $\delta^{18}O$ values of quartz range from 13.8 to 17.9‰ (avg. 15.0‰) for vein I and from 13.3 to 15.2‰ (avg. 14.1‰) for vein II. The $\delta^{18}O$ values of water equilibrated with quartz were calculated using the estimated trapping temperature of primary type IV fluid inclusions and oxygen isotope fractionation equation for quartz-water from Zheng (1993). The results are between 9.6 and 13.7‰ (avg. 10.8‰) for vein I and between 9.1 and 10.9‰ (avg. 9.9‰) for vein II. The δD values of inclusion waters are between –76 and –68‰ (avg. –71‰) for the prograde stage and between –73 and –67‰ (avg. –69‰) for the retrograde stage in vein I, and the δD values for the prograde stage in vein II range from –86 to –78‰ (avg. –82‰). The $\delta^{13}C_{CO2}$ values of inclusion fluids range from 0.1 to 2.4‰ (avg. 1.0‰) for vein I and from –3.5 to –1.7‰ (avg. –2.5‰) for vein II.

Interpretation of oxygen, carbon, and hydrogen isotope data

Shin and Lee (2003) reported that $\delta^{13}C$ values of calcite from the skarn in the Poongjeon deposit range from –5.1 to –4.2‰, which is within the range of CO_2 values commonly found in granitic rocks (Taylor and Friedrichsen, 1983). Because the $\delta^{13}C$ values of the inclusion fluids in vein I, ranging from 0.1 to 2.4‰, are higher than those of skarn calcite, there is a possibility of an external contribution to the primary magmatic fluid. It is known that CO_2 liberated from decarbonation of carbonates during contact metamorphism is much richer in ^{18}O and ^{13}C than the original carbonates (Valley, 1986). Thus, the most plausible explanation is that there was an involvement of ^{13}C-enriched fluids produced from decarbonation reaction that resulted in the formation of abundant calc-silicate minerals. The decarbonated fluids must have utilized fractures, faults, lithologic contacts and reaction-enhanced permeability to have an isotopic exchange with magmatic fluids that could infiltrate the system.

Carbon isotope compositions, –3.5 to –1.7‰, of CO_2 from CH_4-rich inclusion fluids in vein II are lower than those of fluids from vein I (Fig. 11). According to previous discussions, the following possibilities may be suggested for the lower isotope values: either a more intensive effect of magmatic fluids or the strong effect of metasediment-derived fluids. It is, however, unlikely that magmatic carbons were introduced preferably into the contact between amphibolite and metapelite rather than into major fault zones or other geologic contacts. Instead, as indicated by the abundance of CH_4-rich fluid inclusions in vein II, the metasediment-derived fluids, in addition to magmatic fluids and decarbonated fluids, which provided organic carbons commonly with ^{13}C-depleted CO_2, –14 to –1‰ (Botz *et al*., 2002; Fiebig *et al*., 2004), may have made important contributions to lowering the

$\delta^{13}C$ values of vein II inclusion fluids.

Most of the $\delta^{18}O_{H2O}$ values of vein I and II belong to the magmatic water range (Fig. 12). Similar to $\delta^{13}C_{CO2}$ values, the higher $\delta^{18}O_{H2O}$ values of vein I than those of vein II could have resulted from the effect of ^{18}O-enriched fluids produced from decarbonation reaction. Hydrogen isotope compositions of inclusion fluids in vein I, which belong to the magmatic water range of the Muamsa Granite, –78 to –56‰ (Shin and Lee, 2003), remained fairly constant from prograde to retrograde stage (Table 2). This accords with the interpretation that talc mineralization was typically influenced by magmatic fluids as demonstrated by oxygen and hydrogen isotope compositions of talc ores (Park *et al*., 1997).

The lower δD values of vein II fluids relative to those of vein I fluids should be explained. Meteoric water models for numerous hydrothermal ore deposits have been adequate to explain low but variable δD values of mineralizing fluids (e.g., Shelton *et al*., 1988; Tornos and Spiro, 2000). However, these models cannot be successfully applied to the Poongjeon deposit because water-rock interaction by the passage of local meteoric waters through major fault zones or the contacts between different rock units in the same geologic pile cannot reasonably explain the large difference (of about 11‰) in δD values between the two quartz types. The abundance of type IVB inclusions also mitigates the possibility of the contribution of meteoric water to lower δD values of vein II inclusion fluids.

Instead, the lower δD values may reflect fractionation effects between water and other gases, mostly CH_4 (Horibe and Craig, 1995; So and Yun, 1997), because it has been reported that hydrogen isotope compositions of methane derived from organic matter and/or graphite range from –250 to –90‰ (Sheppard, 1986; Schimmelmann *et al*., 1999). Similar to the depleted carbon isotope compositions of vein II, it seems likely that the magmatic fluids have circulated the metasedimentary rocks and contributed to lowering δD values of vein II inclusion fluids. However, due to the lack of original δD values of methane related to the metasedimentary rocks, it is difficult to estimate quantitatively how much of a contribution methane has made to the hydrogen isotopic compositions of the inclusion fluids.

Genetic Constraints of Talc

It should be noted that though the trapping temperature of secondary type IVB inclusions, 260° to 315°C, provides the appropriate lower limit of the talc formation, the upper limit can be higher than 315°C as discussed above about the trapping condition of fluid inclusions. From T-X_{CO2} diagram representing the variation of mineral assemblages in the marble during the contact metamorphism, Shin and Lee (2002) demonstrated that most talc in the Poongjeon deposit started to grow as an alteration product of tremolite at temperatures less than 390°C with $X_{CO2} < 0.01$. Thus the fluid inclusion data combined with T-X_{CO2} diagram provide more restricted talc-forming temperature between 260° and 390°C with pressures mostly below 700 bars.

Some carbonate-hosted talc deposits of hydrothermal alteration origin around the world show similar formational conditions (e.g., temperature, pressure, X_{CO2}, structural setting, etc.) to the Poongjeon deposit. Talc deposits in the Ruby Range, Montana, formed with infiltration of seawater which circulated along faults, folds, and contacts between marble and gneiss, where the heated seawater by the anomalous crustal geotherm came into contact with calcite marble, dolomitized the marble, and then converted it to talc at temperature between 250° and 350°C (Brady *et al*., 1998). Oxygen and carbon isotope study suggested that the metasomatic fluids were oxygen-rich and carbon-poor, namely water-rich and CO_2-poor as talc mineralization requires a large volume of water.

The talc deposits of Puebla de Lillo, Iberia, formed in the temperature range of 280° to 405°C at pressure from 165 to 450 bars (Tornos and Spiro, 2000). The mineralizing fluids were CO_2-poor ($X_{CO2} \approx 0.003$–0.01) and saline brines (up to 23 wt.% NaCl equiv.) of NaCl-$MgCl_2$-$CaCl_2$-KCl system that has isotope compositions of $\delta^{18}O \approx 5.0$–7.9‰ and $\delta D \approx -72$‰. They were produced by mixing of deep brines and meteoric waters with the proportion of the latter increasing with time and were channeled along extensional structures. Talc mineralization at Göpfersgrün in Germany also occurred at low $X_{CO2} \approx 0.05$ and at temperatures between 250 and 400°C by hydrothermal alteration of dolomitic marble along a major fault zone (Hecht *et al*., 1999).

Similarly to the Poongjeon deposit, talc minerals hosted by impure dolomitic limestone in the Atshan deposit in Egypt were produced as a secondary phase during the retrograde stage of contact metamorphism (Schandl *et al*., 1999), though their precursor minerals are different with each other due to their different host-rock compositions and fluid evolution histories (Shin and Lee, 2002).

Summary

Geochemical data of fluid inclusions indicate that fluid evolution related to talc mineralization in the Poongjeon deposit is characterized by two different types of quartz veins. Boiling of carbonaceous fluids producing high X_{CO2} fluids and aqueous or low X_{CO2} fluids and mixing of halite ± sylvite-bearing fluids with carbonaceous fluids are major processes in vein I. In the mean time, the coexist-

ence of $CH_4 \pm H_2O$, H_2O-CO_2-CH_4 fluid inclusions with variable CH_4/CO_2 ratios, and high X_{CO2} fluid inclusions in vein II are the products of fluid mixing.

Occurrences of halite ± sylvite-bearing inclusions of magmatic origin along trails as secondary phase are closely related to the talc mineralization and their entrapment conditions are estimated to be between 150 and 700 bars at 260°–390°C.

The $\delta^{13}C_{CO2}$ values, 0.1–2.4‰, of inclusion fluids of vein I and lower $\delta^{13}C_{CO2}$ values, –3.5 to –1.7‰, of vein II suggest that CO_2 liberated from the decarbonation for calc-silicate formation and from metasediment-derived fluids during the prograde stage of the contact metamorphism were mixed up respectively with magmatic fluids in each vein system. Higher $\delta^{18}O_{H2O}$ values of vein I and lower δD values of vein II seem to have similar evolutionary histories as $\delta^{13}C$ values. Geologic structures such as faults and contacts between different rock units seem to have promoted infiltration, mixing, and unmixing of fluids of diverse origins.

Acknowledgments—This work was supported by the Post-doctoral Fellowship Program of Korea Science & Engineering Foundation (KOSEF). We also acknowledge a partial support from the Korea Institute of Geoscience and Mineral Resources. The critical reviews by two anonymous reviewers substantially improved this contribution and are greatly appreciated.

REFERENCES

Anderson, M. R., Rankin, A. H. and Spiro, B. (1992) Fluid mixing in the generation of mesothermal gold mineralization in the Transvaal Sequence, Transvaal, South Africa. *Eur. J. Mineral.* **4**, 933–948.

Bodnar, R. J. (1993) Revised equation and table for determining the freezing point depression of H_2O-NaCl solutions. *Geochim. Cosmochim. Acta* **57**, 683–684.

Bodnar, R. J., Sterner, S. M. and Hall, D. L. (1989) SALTY: a fortran program to calculate compositions of fluid inclusions in the system NaCl-KCl-H_2O. *Computers & Geosciences* **15**, 19–41.

Botz, R., Wehner, H., Schmitt, M., Worthington, T. J., Schmidt, M. and Stoffers, P. (2002) Thermogenic hydrocarbons from the offshore Calypso hydrothermal field, Bay of Plenty, New Zealand. *Chem. Geol.* **186**, 235–248.

Bowers, T. S. and Helgeson, H. C. (1983a) Calculation of the thermodynamic and geochemical consequences of nonideal mixing in the system H_2O-CO_2-NaCl on phase relations in geologic systems: Equation of state for H_2O-CO_2-NaCl fluids at high pressures and temperatures. *Geochim. Cosmochim. Acta* **47**, 1247–1275.

Bowers, T. S. and Helgeson, H. C. (1983b) Calculation of the thermodynamic and geochemical consequences of nonideal mixing in the system H_2O-CO_2-NaCl on phase relations in geologic systems: metamorphic equilibria at high pressures and temperatures. *Am. Mineral.* **68**, 1059–1075.

Brady, J. B., Cheney, J. T., Rhodes, A. L., Vasquez, A., Green, C., Duvall, M., Kogut, A., Kaufman, L. and Kovaric, D. (1998) Isotope geochemistry of Proterozoic talc occurrences in Archean marbles of the Ruby Mountains, southwest Montana, U.S.A. *Geol. Material Res.* **1**, 1–41.

Burnham, C. W. and Ohmoto, H. (1980) Late stage processes of felsic magmatism. *Min. Geol. Spec.* **8**, 1–11.

Burrus, R. C. (1981) Analysis of phase equilibria in C-O-H-S fluid inclusions. *MAC Short Course in Fluid Inclusions: Applications to Petrology* (Hollister, L. S. and Crawford, M. L., eds.), Mineral. Assoc. Canada, Toronto, **6**, 39–74.

Clayton, R. N. and Mayeda, T. K. (1963) The use of bromine pentafluoride in the extraction of oxygen from oxides and silicates for isotopic analysis. *Geochim. Cosmochim. Acta* **27**, 43–52.

Cline, J. S. and Bodnar, R. J. (1994) Direct evolution of brine from a crystallizing silicic melt at the Questa, New Mexico, molybdenum deposit. *Econ. Geol.* **89**, 1780–1802.

Cluzel, D., Cadet, J. P. and Lapierre, H. (1990) Geodynamics of the Ogcheon Belt (South Korea). *Tectonophysics* **183**, 41–56.

Collins, P. L. F. (1979) Gas hydrates in CO_2-bearing inclusions and the use of freezing data for estimation of salinity. *Econ. Geol.* **74**, 1435–1444.

Darling, R. S. (1991) An extended equation to calculate NaCl contents from final clathrate melting temperatures in H_2O-CO_2-NaCl fluid inclusions: Implications for P-T isochore location. *Geochim. Cosmochim. Acta* **55**, 3869–3871.

Diamond, L. W. (1992) Stability of CO_2 clathrate hydrate + CO_2 liquid + CO_2 vapour + aqueous KCl-NaCl solutions: Experimental determination and application to salinity estimates of fluid inclusions. *Geochim. Cosmochim. Acta* **56**, 273–280.

Fan, H-R., Groves, D. I., Mikucki, E. J. and McNaughton, N. J. (2000) Contrasting fluid types at the Nevoria gold deposit in the Southern Cross greenstone belt, western Australia: Implications of auriferous fluids depositing ores within an Archean banded iron-formation. *Econ. Geol.* **95**, 1527–1536.

Ferry, J. M. and Burt, D. M. (1982) Characterization of metamorphic fluid composition through mineral equilibria. *Characterization of Metamorphism through Mineral Equilibria* (Ferry, J. M., ed.), Reviews in Mineralogy **10**, 207–262.

Fiebig, J., Chiodini, G., Caliro, S., Rizzo, A., Spangenberg, J. and Hunziker, J. C. (2004) Chemical and isotopic equilibrium between CO_2 and CH_4 in fumarolic gas discharges: Generation of CH_4 in arc magmatic-hydrothermal systems. *Geochim. Cosmochim. Acta* **68**, 2321–2334.

Fu, B., Williams, P. J., Oliver, N. H. S., Dong, G., Pollard, P. J. and Mark, G. M. (2003) Fluid mixing versus unmixing as an ore-forming process in the Cloncurry Fe-oxide-Cu-Au District, NW Queensland, Australia: evidence from fluid inclusions. *J. Geochem. Exp.* **78–79**, 617–622.

Hecht, L., Freiberger, R., Gilg, H. A., Grundmann, G. and Kostitsyn, Y. A. (1999) Rare earth element and isotope (C, O, Sr) characteristics of hydrothermal carbonates: genetic implications for dolomite-hosted talc mineralization at Göpfersgrün (Fichtelgebirge, Germany). *Chem. Geol.* **155**, 115–130.

Horibe, Y. and Craig, H. (1995) D/H fractionation in the system methane-hydrogen-water. *Geochim. Cosmochim. Acta* **59**, 5209–5217.

Ishihara, S. (1981) The granitoid series and mineralization. *Econ. Geol. Anniv.* **75**, 458–484.

Jang, B. A. and Gim, J. A. (1996) Cretaceous paleostress from healed microcracks and fluid inclusions in granites from the Sogrisan and the Wolagsan area. *J. Geol. Soc. Korea* **32**, 291–301 (in Korean).

Jin, M. S. (1985) A relationship between tectonic setting and chemical composition of the Cretaceous granitic rocks in southern Korea. *J. Geol. Soc. Korea* **21**, 67–73.

Jin, M. S., Choo, S. H., Chi, S. J., Kim, S. J. and Shin, S. C. (1992) Radiometric ages of the Paleozoic and Mesozoic granites in the middle part of the Ogcheon Fold Belt. *Researches on Isotope Geology*, Korea Institute of Geology, Mining and Materials **KR-92-1G-2-1**, 1–34 (in Korean).

KMPC (1989) Investigation Report of Ore Deposits Drilling. *Korea Mining Promotion Corporation* **12**, 387–479 (in Korean).

Lee, S. H. and Choi, G. J. (1994) Phase equilibria between coexisting minerals in the talc ores and process of talc formation in the Daeheung talc deposits, Korea. *J. Petrol. Soc. Korea* **3**, 156–170 (in Korean).

Molnar, F., Watkinson, D. H. and Everest, J. O. (1999) Fluid-inclusion characteristics of hydrothermal Cu-Ni-PGE veins in granitic and metavolcanic rocks at the contact of the Little Stobie deposit, Sudbury, Canada. *Chem. Geol.* **154**, 279–301.

Newberry, R. J. (1982) Tungsten-bearing skarns of Sierra Nevada. I. The Pine Creek mine, California. *Econ. Geol.* **77**, 823–844.

Park, H. I., Lee, I. S., Hur, S. D. and Shin, D. B. (1997) Talc mineralization in the middle Ogcheon metamorphic belt (II): Poongjeon talc deposit. *Econ. Environ. Geol.* **30**, 543–551 (in Korean).

Rios, F. J., Villas, R. N. and Fuzikawa, K. (2003) Fluid evolution in the Pedra Preta wolframite ore deposit, Paleoproterozoic Musa granite, eastern Amazon craton, Brazil. *J. South Am. Earth Sci.* **15**, 787–802.

Roedder, E. (1984) The origin of fluid inclusions. *Fluid Inclusions* (Roedder, E., ed.), Reviews in Mineralogy **12**, 11–45.

Schandl, E. S., Sharara, N. A. and Gorton, M. P. (1999) The origin of the Atshan talc deposit in the Hamata area, eastern desert, Egypt: A geochemical and mineralogical study. *Can. Mineral.* **37**, 1211–1227.

Schimmelmann, A., Lewan, M. D. and Wintsch, R. P. (1999) D/H isotope ratios of kerogen, bitumen, oil, and water in hydrous pyrolysis of source rocks containing kerogen types I, II, IIS, and III. *Geochim. Cosmochim. Acta* **63**, 3751–3766.

Seitz, J. C. and Pasteris, J. D. (1990) Theoretical and practical aspects of differential partitioning of gases by clathrate hydrates in fluid inclusions. *Geochim. Cosmochim. Acta* **54**, 631–639.

Selby, D., Nesbitt, B. E., Muehlenbachs, K. and Prochaska, W. (2000) Hydrothermal alteration and fluid chemistry of the Endako Porphyry Molybdenum Deposit, British Columbia. *Econ. Geol.* **95**, 183–202.

Shelton, K. L., So, C. S. and Chang, J-S. (1988) Gold-rich mesothermal vein deposits of the Republic of Korea: Geochemical studies of the Jungwon Gold area. *Econ. Geol.* **83**, 1221–1237.

Sheppard, S. M. F. (1986) Characterization and isotope variations in natural waters. *Stable Isotopes* (Valley, J. W., Taylor, H. P., Jr. and O'Neil, J. R., eds.), Reviews in Mineralogy **16**, 165–183.

Shin, D. B. and Lee, I. S. (2000) Geochemical study on the host rocks of the Poongjeon talc deposits, Korea: Implication for the source rock. *J. Geol. Soc. Korea* **36**, 235–248 (in Korean).

Shin, D. B. and Lee, I. S. (2002) Carbonate-Hosted Talc Deposits in the Contact Aureole of Igneous Intrusion (Hwanggangri Mineralized Zone, South Korea): geochemistry, phase relationships, and stable isotope studies. *Ore Geol. Rev.* **22**, 17–39.

Shin, D. B. and Lee, I. S. (2003) Evaluation of the volatilization and infiltration effects on the stable isotopic and mineralogical variations in the carbonate rocks adjacent to the Cretaceous Muamsa Granite, South Korea. *J. Asian Earth Sci.* **22**, 227–243.

So, C. S. and Yun, S. T. (1992) Geochemistry and genesis of hydrothermal Au-Ag-Pb-Zn deposits in the Hwanggangri mineralized district, Republic of Korea. *Econ. Geol.* **87**, 2056–2084.

So, C. S. and Yun, S. T. (1994) Origin and evolution of W-Mo-producing fluids in a granitic hydrothermal system: Geochemical studies of quartz vein deposits around the Susan granite, Hwanggangri district, Republic of Korea. *Econ. Geol.* **89**, 246–267.

So, C. S. and Yun, S. T. (1997) Jurassic Mesothermal gold mineralization of the Samhwanghak Mine, Youngdong Area, Republic of Korea: Constraints on hydrothermal fluid geochemistry. *Econ. Geol.* **92**, 60–80.

Taylor, B. E. and Friedrichsen, H. (1983) Light stable isotope systematics of granitic pegmatites from North America and Norway. *Isotope Geoscience* **1**, 127–167.

Taylor, H. P., Jr. and Sheppard, S. M. F. (1986) Igneous rocks: I. Process of isotopic fractionation and isotope systematics. *Stable Isotopes in High Temperature Geological Processes* (Valley, J. W., Taylor, H. P., Jr. and O'Neil, J. R., eds.), Reviews in Mineralogy **16**, 227–271.

Thiery, R., Van den Kerkhof, A. M. and Dubessy, J. (1994) *v*X properties of CH_4-CO_2 and CO_2-N_2 fluid inclusions: modelling for T < 31°C and P < 400 bars. *Eur. J. Mineral.* **6**, 753–771.

Tornos, F. and Spiro, B. F. (2000) The geology and isotope geochemistry of the talc deposits of Puebla de Lillo (Cantabrian Zone, Northern Spain). *Econ. Geol.* **95**, 1277–1296.

Tritlla, J. and Cardellach, E. (1997) Fluid inclusions in pre-ore minerals from the carbonate-hosted mercury deposits in the Espadan Ranges (eastern Spain). *Chem. Geol.* **137**, 91–106.

Turner, F. J. (1935) Geological investigations of the nephrites, serpentines, and related "green stones" used by the Maoris of Otago and South Canterbury. *Royal Soc. New Zealand, Trans. Proc.* **65**, 187–210.

Valley, J. W. (1986) Stable isotope geochemistry of metamor-

phic rocks. *Stable Isotopes in High Temperature Geological Processes* (Valley, J. W., Taylor, H. P., Jr. and O'Neil, J. R., eds.), Reviews in Mineralogy **16**, 445–489.

Van den Kerkhof, A. M. and Thiery, R. (1994) Phase transitions and density calculation in the CH_4-CO_2-N_2 system. *Fluid Inclusions in Minerals, Methods and Application* (De Vivo, B. and Frezzotti, M. L., eds.), International Mineralogical Association Working Group, Pontignano-Siena, Short Course Handbook, 171–190.

Zheng, Y. F. (1993) Calculation of oxygen isotope fractionation in anhydrous silicate minerals. *Geochim. Cosmochim. Acta* **57**, 1079–1091.